Eur. Phys. J. C (2025) 85:1402
https://doi.org/10.1140/epjc/s10052-025-15159-w

THE EUROPEAN PHYSICAL JOURNAL C

Check for updates

Regular Article - Theoretical Physics

Einasto-core generalization of the Dymnikova regular black hole metric

Mohammad Alshammari[1,a], **Saleh Alshammari**[1,b], **S. Khan**[2,c], **M. Mossa Al-sawalha**[1,d]

[1] Department of Mathematics, College of Science, University of Ha'il, 2440 Ha'il, Saudi Arabia
[2] University of Agriculture Faisalabad, Constituent College, Toba Tek Singh 36050, Pakistan

Received: 27 October 2025 / Accepted: 2 December 2025
© The Author(s) 2025

Abstract In this work, we develop an Einasto-core generalization of the Dymnikova regular black hole metric, motivated by the flat density profile and the Einasto-type density distribution used in modeling dark matter halos and galactic structures. Replacing the exponential source term in the Dymnikova metric with an Einasto-type profile defined by the parameter α, we obtain a new, regular class of asymptotically flat and spherically symmetric configurations. We derive the corresponding spacetime metric by employing the Einstein field equations with an anisotropic stress-energy tensor as the matter source. Our analysis confirms that a family of regular black hole solutions can be constructed for arbitrary values of the Einasto index α and for a broad range of mass parameters M.The resulting configuration smoothly interpolates between a de Sitter core at the center and a Schwarzschild-like exterior at large radii, preserving the regular character of the geometry. It is observed that the interpolation of different shape parameter values leads to distinct self-gravitational, anisotropic populations of cosmic objects with unique physical characteristics. The non-singular and viable nature of the obtained solution is examined through the finiteness of the scalar curvature.

1 Introduction

The theoretical framework of the cold dark matter (CDM) model for the evolution of cosmological entities is firmly established and demonstrates excellent agreement with observations on astrophysical scales [1]. The CDM model frequently involves massive particles that interact weakly (WIMPs). Their interaction cross-section, characteristic of weak interactions, yields the correct relic abundance if these particles were in thermal equilibrium in the early universe. Astrophysically, WIMP-based self-gravitational halo entities exhibit several micro-scale inconsistencies. These include the cusp–core issue, the overabundance of observed subhaloes, the diversity in observed rotation curves and stellar distributions, and dynamical discrepancies exemplified by the "too-big-to-fail" [2]. The abundance of dark matter (DM) in the cosmic budget implies that the universe is densely populated with DM haloes. To understand the population of halo configurations in the cosmos, several density distributions have been analyzed in the literature. Describing the density distribution of dark matter (DM) haloes is typically initiated using the Navarro, Frenk, and White [3]. This model is considered fundamental for characterizing the DM distribution. Characterized by two distinct power laws, the NFW density distribution has an inner density slope of r^{-1} and an outer slope that decays as r^{-3}. It represents a special case of double power law models, with asymptotic slopes $r^{-\gamma}$ and $r^{-\beta}$ that describe the behavior of inner and outer density. Beyond the NFW model, several heuristic profiles have been developed, including the Moore [4], DC14 [5], and Burkert [6] forms, as well as luminous matter distributions such as the de Vaucouleurs [7] and Jaffe [8] profiles. In this respect, Khan and Mahmoud [9] examined the possible connection between central galactic black holes and DM using the multi-parameter Zhao density distribution using the Hu-Sawicki $f(R)$ gravity. Although these profiles are inspired by analytical insights, their exact functional representations have been refined through cosmological N-body simulations [3]. Lacking a derivation from fundamental physical principles, it is still unclear why these empirical density profiles provide such good agreement with numerical simulations and observational data. Only a limited number of studies have attempted to derive these density profiles through a statisti-

[a] e-mail: dar.alshammari@uoh.edu.sa
[b] e-mail: saleh.alshammari@uoh.edu.sa
[c] e-mail: suraj.pu.edu.pk@gmail.com (corresponding author)
[d] e-mail: m.alswalha@uoh.edu.sa

Published online: 10 December 2025

cal framework [10]. The dynamical and gravitational lensing characteristics of this family of double power-law models have been extensively studied in the literature [11–13].

Even though the existence of cosmic DM is confirmed by a variety of discoveries, its fundamental particle composition remains a significant obstacle that connects particle physics and stellar astronomy [14]. A wide variety of DM candidates with masses spanning many orders of magnitude have been proposed. In this context, Fuzzy dark matter (FDM) serves as an interesting and appealing modification of the CDM framework, maintaining consistency with cosmological structures while addressing several long-standing small-scale issues [15,16]. FDM assumes that light bosons constitute DM and predicts the formation of a solitonic core, often referred to as a boson star, stabilized by wave pressure at the center of halos. This is based on ultralight axions as a means to resolve the galactic-scale discrepancies inherent in the CDM framework. FDM wave interference produces density fluctuations capable of perturbing the motion of a supermassive galactic object at the center of its host halo. FDM exhibits a distinctive behavior at subatomic scales, which contrasts with the classical CDM model. However, FDM retains the extraordinary outcomes of the CDM cosmological model because the findings are consistent with CDM at astrophysical scales. In the fuzzy dark matter (FDM) framework, dark matter is modeled as an ultralight bosonic field with a particle mass ranging from 10^{-23} to 10^{-21} eV.

Structures formed by these particles exhibit a central core enclosed by an outer envelope with a profile analogous to that of CDM. The core itself serves as a characteristic hallmark of the FDM model, as demonstrated by structure formation simulations [17–20]. Detailed studies of core formation at small scales have been conducted mainly in two simulation settings. The first corresponds to the multi-merging of cores, as examined in the studies [18,21], resulting in the emergence of core–halo configurations. A second scenario considers kinetic relaxation from random initial conditions as the mechanism driving core formation [22,23]. The existence of black holes and how they behave within FDM cores is a crucial component added to FDM phenomenology.

Navarro et al. [24] and Merritt et al. [25] proposed an alternative model in which the logarithmic density slope, rather than the density, exhibits a power-law dependence. This formulation was shown to reproduce the density structure of high-resolution N-body DM haloes more accurately than the NFW profile. The idea of representing a system through a power-law logarithmic density slope was first proposed by Einasto [26], who applied it to model stellar distributions in nearby galaxies such as M 31, M 32, M 87, and later in the Milky Way [27], forming the basis of what is now known as the Einasto profile. Unlike models where the density follows a power-law form, in this case the logarithmic density slope is the quantity that exhibits a power-law behavior. N-body simulations of ΛCDM [24] reveal that the Einasto density distribution [26,27] yields an excellent universal fit for DM haloes spanning a wide mass range. The physical and dynamical properties of the Einasto model have been extensively investigated by several authors [28–32]. Recent astrophysical research has highlighted the significance of dark matter and the constraint of a vanishing gravitational complexity factor in shaping the formation processes and physical characteristics of anisotropic compact stars [33–39].

To tackle the fundamental issues encountered in Einstein's classical model at the Planck scale, noncommutative geometry (NCG) provides a compelling framework for describing FDM-based galactic halos. The center singularity, the area of formal spacetime curvature divergence typical of classical black hole solutions, is avoided by this approach, which is its main significance. A minimal length scale, represented by the parameter θ, is naturally produced by NCG-inspired models, which consider spacetime coordinates as non-commuting operators. NCG is characterized by the noncommutation of the spacetime coordinate operators, expressed as follows: $[\hat{x}^{\mu}, \hat{x}^{\nu}] = i\,\theta^{\mu\nu}$, where $\hat{x}^{\mu}$ is an antisymmetric matrix. In addition, NCG alters black hole thermodynamics by modifying the Hawking temperature and entropy, typically leading to the prediction of a remnant with a minimum mass. The existence of a minimum mass suggests that Hawking evaporation may stop, resulting in a stable black hole remnant and potentially addressing the information loss paradox. Some models, such as the $(2+1)$-dimensional fuzzy BTZ black hole, realize fuzzy black holes as quantum spaces described by a noncommutative operator algebra, where the horizon and interior arise from the quantum geometry, linking NCG to the quantum nature of gravity. The Gaussian distribution is a special case of what is known as the Einasto profile of DM, connecting fuzzy black hole models to broader astrophysical density profiles. In the context of NCG, Khan and Yousaf [40,41] proposed fuzzy black hole–like configurations by merging a de Sitter–type core with the Einasto-type density distribution in $f(R)$ gravity. For further applications of NCG in modified theories of gravity, one may refer to astrophysical investigations examining the influence of NCG on anisotropic stellar models of compact stars [42–46].

In relativistic astrophysics, the modeling of astrophysical stellar configurations has increasingly focused on the effects of pressure anisotropy, which arises when the principal stresses $(p_r, p_\perp)$ differ from each other, i.e., pressure is direction-dependent. Although early relativistic models often treated stellar interiors as isotropic perfect fluids, it is now recognized that at densities exceeding nuclear matter, deviations from isotropy become significant. The degree of anisotropy is quantified by the factor $\Delta := p_r - p_\perp$, which strongly influences the equilibrium configuration, stability, and maximum mass of the star. Pressure anisotropy is commonly introduced in models of self-gravitating fluids because

it occurs in numerous physically meaningful contexts [47]. It has also been shown [48] that pressure anisotropy inevitably arises during stellar evolution, even when a system is initially modeled as isotropic. Anisotropic pressures can modify the gravitational field, alter the energy density profile, and lead to a range of rich relativistic phenomena, including changes in central density, phase transitions [49,50], and novel structural features. The relevance of unequal principal stresses is highly significant for understanding the astrophysical framework of compact formations when employing different gravity models in stellar astronomy. Owing to its applications in astrophysics, a novel anisotropic solution describing the hybrid star configuration based on the MIT model was developed by et al. [51]. Their research explored the governing influence of complexity-free conditions on the dynamics of hybrid-matter compact objects. To stay up-to-date with recent astronomical studies on the relativistic analysis of stellar objects, several contemporary investigations should be incorporated [52–56].

In this study, we examine the geometric and physical characteristics of the fuzzified Dymnikova metric by generalizing it through the Einasto density distribution. The corresponding spacetime metric is derived, and the behavior of curvature invariants, energy conditions, and the effective potential is analyzed. Particular emphasis is placed on the role of the Einasto index in regulating the degree of regularity and determining the characteristic scales of the black hole solution, thereby extending Dymnikova's model into a broader and more versatile relativistic framework. The paper proceeds as follows. Section 2 reviews the Einasto density distribution and the corresponding essential formulae. Section 3 focuses on the construction of the fuzzified Dymnikova black hole metric. Section 4 is devoted to the analysis of the energy conditions for the proposed model. In Sect. 5, we examine the effective potentials corresponding to the present solution and the Schwarzschild metric for comparison. Finally, the conclusions are summarized in Sect. 6.

2 The Einasto-type density distribution

For describing radial variations in the density of dense-matter configurations, the Einasto-type model offers an empirical and flexible parametrization. Unlike the standard isothermal or NFW profiles, the Einasto profile incorporates an exponential element that allows for a continually fluctuating logarithmic slope, providing a more flexible representation of galactic and stellar structures [24,57,58]. According to Einasto, any astrophysical model that is theoretically coherent needs to include describing functions [59]. These functions, which jointly obey a well-defined set of restrictions, include the density, effective potential, and mass function. Since they are integrals of the underlying density distribution, all the describing functions can be traced back to the form of $\sigma(r)$. It is thus evident that the density profile serves as the dominant functional form in describing the structure of a galactic system, and It is expected to comply with the following physical criteria: The density function $\rho = \rho(r)$ must satisfy the following fundamental requirements:

(a) $\sigma : \mathbb{R}_+ \to [0, \infty)$, with $\sigma(r) < \infty \; \forall r > 0$.
(b) $\sigma \in C^\infty(\mathbb{R}_+)$, $\sigma'(r) \leq 0 \; \forall r > 0$, $\lim_{r\to\infty} \sigma(r) = 0$, where $f' := \partial_r f$.
(c) The finiteness of specific moments of the mass profile, namely those associated with the central gravitational potential, the total mass, and the effective (mean) radius, is a necessary condition for a physically acceptable model.
(d) All descriptive functions $f(r)$ derived from $\sigma(r)$ must remain continuous throughout $\mathbb{R}_+$; that is,

$$f \in C^0(\mathbb{R}_+),$$

ensuring that no jump discontinuities occur within the physical domain.

Over the years, the DM Einasto-type density distribution has found extensive application in modeling diverse galactic systems, such as spherical, elliptical, and disc galaxies, as well as in describing the internal density structure of DM halos [24,28,29,57,60]. For recent analytical investigations of the Einasto model in modeling DM-based self-gravitating compact configurations see [33,61–65]. The Einasto profile is distinguished by a power law form of the logarithmic slope of the density distribution

$$\frac{d\ln\sigma}{d\ln r} \propto r^\alpha, \tag{1}$$

where α is a dimensionless shape parameter determining the rate at which the slope changes with r. Alternatively, one may express it explicitly as

$$\frac{d\ln\sigma}{d\ln r} = -2\left(\frac{r}{r_{-2}}\right)^\alpha, \tag{2}$$

where r_{-2} denotes the radius at which the logarithmic slope equals -2. Integrating this relation yields the Einasto-type density distribution:

$$\sigma(r) = \sigma_{-2}\exp\left[-\frac{2}{\alpha}\left(\left(\frac{r}{r_{-2}}\right)^\alpha - 1\right)\right], \tag{3}$$

where σ_{-2} is the density at $r = r_{-2}$.

To obtain a simplified exponential form, we redefine the constants as

$$\sigma_0 = \sigma_{-2}e^{\frac{2}{\alpha}}, \qquad h = r_{-2}\left(\frac{\alpha}{2}\right)^{\frac{1}{\alpha}}. \tag{4}$$

Substituting these into Eq. (3), the profile reduces to

$$\sigma(r) = \sigma_0 \exp\left[-\left(\frac{r}{h}\right)^{\frac{1}{\alpha}}\right], \tag{5}$$

where σ_0 is the central density and h is a characteristic scale radius.

In such multi-component models, each structural component is described by an individual parameter set $\{\sigma_0,\ h,\ \alpha\}$, which represents a distinct, physically homogeneous galactic configuration. Navarro et al. [24] reported that, for haloes spanning a wide mass range from dwarf galaxies to galaxy clusters, the Einasto shape parameter α varies between 4.54 and 8.33, with an average value of $\alpha = 5.88$. Furthermore, according to Gao et al. [66] that the most massive halos in the Millennium Run are characterized by the Einasto index $\alpha \approx 4.35$. Using the Einasto profile, Chemin et al. [60] analyzed the rotation curves of spiral galaxies from the THINGS survey and found that the Einasto index α tends to be smaller by a factor of two or more than that inferred from N-body simulations. Furthermore, Hayashi and White [57] and Gao et al. [66] showed that the Einasto shape parameter n decreases with both halo mass and redshift, taking values of about $\alpha \approx 5.88$ for galaxy-sized haloes and $\alpha \approx 4.35$ for cluster-sized haloes in the Millennium Run simulation [67]. Employing a multi-parameter Einasto method, the authors of [68] fitted the surface brightness profiles of many elliptical galaxies in the Virgo cluster, assigning two or three components per galaxy, with each component described by a distinct α value. In the central component, α tends to be around 1 for the most massive and shallow-cusp galaxies, whereas it remains below 2 for steep-cusp galaxies. On the other hand, the outer component of massive galaxies is characterized by α values between 5 and 8. For the astrophysical dark matter structures ($\alpha = 7.072$, $h = 2.121 \times 10^{-9}$ kpc, $M = 4.57 \times 10^9 M_\odot$ [27,59]), the central radial pressure takes the value $|p_r(0)| \sim 5.8 \times 10^{-41}\ \mathrm{m}^{-2}$ in geometric units, or alternatively $|p_r(0)| \sim 7 \times 10^3\ \mathrm{N/m^2}$ in SI units.

Now, we compute the mass of the Einasto-type DM distribution using the general relativistic expression

$$M(r)' = 4\pi r^2 \sigma(r), \tag{6}$$

which upon substituting the density form (5), we get

$$M(r) = 4\pi\sigma_0 \int_0^\infty \exp\left[-\left(\frac{r}{h}\right)^{\frac{1}{\alpha}}\right] z^2 d(z), \tag{7}$$

whose solution reads

$$M(r) = 4\pi\sigma_0 h^3 \alpha \Gamma(3\alpha). \tag{8}$$

From Eqs. (5) and (8), we have

$$\sigma(r) = \frac{M}{4\pi h^3 \alpha \Gamma(3\alpha)} \exp\left[-\left(\frac{r}{h}\right)^{\frac{1}{\alpha}}\right]. \tag{9}$$

Thus, the total mass associated with the system is given as

$$m(r) = \frac{M\gamma(3\alpha, x(r))}{\Gamma(3\alpha)}, \qquad x(r) = \left(\frac{r}{h}\right)^{\frac{1}{\alpha}}, \tag{10}$$

where $\gamma(3\alpha, x(r))$ is the lower incomplete gamma function.

3 Einstein field equations for the fuzzified Dymnikova metric

We consider a static, spherically symmetric spacetime described by the line element

$$ds^2 = f(r)\,dt^2 - \frac{dr^2}{f(r)} - r^2\,(d\theta^2 + \sin^2\theta\, d\phi^2), \tag{11}$$

where the metric potential $f(r)$ is given by

$$f(r) = 1 - \frac{2m}{r}\left\{1 - \exp\left[-\left(\frac{r}{h}\right)^3\right]\right\}. \tag{12}$$

This is known as Dymnikova black hole metric. This metric was proposed by Dymnikova in the 1990s as a regular black hole solution [69]. Dymnikova's regular black-hole construction follows Gliner's hypothesis that replacing the central region with a de Sitter core prevents the formation of a singularity [70,71]. This solution has particular significance since it provides one of the first elegant models of a non-singular black hole, with a de Sitter-like interior effectively matched to an outer Schwarzschild region. Furthermore, later research has demonstrated that it occurs naturally in a variety of quantum-gravity circumstances, including Asymptotically Safe gravity. The authors of [72] demonstrated that the $d = 4$ Dymnikova density profile can be viewed as the gravitational counterpart of the Schwinger effect. Additionally, it was demonstrated in [73,74] that when the Generalized Uncertainty Principle is considered, the Schwinger mechanism gets particular corrections. In light of this, a few of the current writers have investigated wormholes and suggested a Generalized Uncertainty Principle correction to the Dymnikova density profile [75].

3.1 Einstein tensor components

The Einstein field equations are

$$G_{\mu\nu} = 8\pi T_{\mu\nu}, \tag{13}$$

with the energy-momentum tensor of an anisotropic fluid given by

$$T^{\mu}{}_{\nu} = \text{diag}\,[\sigma, -p_r, -p_\perp, -p_\perp]. \tag{14}$$

For the line element (11), the non-vanishing components of $G^{\mu}{}_{\nu}$ are

$$G^{t}{}_{t} = 8\pi T^{t}{}_{t} \Rightarrow \frac{f'(r)}{r} + \frac{f(r)-1}{r^2} = -8\pi\sigma, \tag{15}$$

$$G^{r}{}_{r} = 8\pi T^{r}{}_{r} \Rightarrow \frac{f'(r)}{r} + \frac{f(r)-1}{r^2} = 8\pi p_r, \tag{16}$$

$$G^{\theta}{}_{\theta} = 8\pi T^{\theta}{}_{\theta} \Rightarrow G^{\phi}{}_{\phi} = \frac{1}{2}f''(r) + \frac{f'(r)}{r} = 8\pi p_\perp, \tag{17}$$

with conservation equation

$$p_r' + \frac{f'}{2f}(\sigma + p_r) + \frac{2}{r}(p_r - p_\perp) = 0. \tag{18}$$

Next, imposing the condition $G^{t}{}_{t} = G^{r}{}_{r}$, we have

$$-8\pi\sigma = 8\pi p_r \Rightarrow \sigma = -p_r. \tag{19}$$

Thus, the radial pressure equals the negative of the energy density, representing the familiar relation of a de Sitter-like core.

Finally, the field equations for the fuzzified Dymnikova (Einasto-core) geometry take the final for

$$\sigma(r) = \sigma_0\, e^{-x(r)}, \tag{20}$$

$$p_r(r) = -\sigma(r), \tag{21}$$

$$p_\perp(r) = -\sigma(r) + \frac{r}{2}\sigma'(r), \tag{22}$$

where $\sigma'(r)$ is given by

$$\rho'(r) = -\frac{x(r)}{\alpha r}\,\rho(r), \qquad x(r) = \left(\frac{r}{h}\right)^{1/\alpha}. \tag{23}$$

Therefore, the tangential pressure can be expressed explicitly as

$$p_\perp(r) = -\sigma_0 e^{-x(r)}\left(1 + \frac{x(r)}{2\alpha}\right). \tag{24}$$

Finally, the metric potential is defined as

$$f(r) = 1 - \frac{2M}{r}\frac{\gamma(3\alpha, x(r))}{\Gamma(3\alpha)}, \tag{25}$$

which reproduces to the original Dymnikova metric for $n = \frac{1}{3}$.

3.2 Comparison with Schwarzschild metric and classical Dymnikova metric

In this subsection, we compare the fuzzified Dymnikova metric (25) with the classical Schwarzschild and Dymnikova black holes. For this let uis define

$$m(r) \equiv M\,\frac{\gamma(3\alpha, x(r))}{\Gamma(3\alpha)}. \tag{26}$$

so that the metric (25), cxan be alternatively defined as

$$f(r) = 1 - \frac{2m(r)}{r}, \tag{27}$$

which highlights that the solution is a Schwarzschild-like geometry with a "smeared" mass profile $m(r)$. In the asymptotic limit, where the incomplete gamma fraction approaches unity, the metric function reproduces the standard Schwarzschild form.

$$f_{\text{Sch}}(r) = 1 - \frac{2M}{r}. \tag{28}$$

More precisely,

$$\lim_{r\to\infty}\frac{\gamma(3\alpha, x(r))}{\Gamma(3\alpha)} = 1 \quad \Rightarrow \quad \lim_{r\to\infty} f(r) = f_{\text{Sch}}(r). \tag{29}$$

Therefore, the spacetime approaches the Schwarzschild geometry asymptotically, retaining the same DM mass M. In the vicinity of the origin, the behavior changes significantly. For small values of x, the lower incomplete gamma function admits the expansion $\gamma(s, x) \sim x^s/s$; therefore,

$$\frac{\gamma(3\alpha, x(r))}{\Gamma(3\alpha)} \sim \frac{1}{3\alpha\,\Gamma(3\alpha)}\left(\frac{r}{h}\right)^{3\alpha/n}. \tag{30}$$

Therefore, for $r \ll h$,

$$f(r) \approx 1 - 2MK\, r^{\frac{3\alpha}{n}-1}, \quad K \equiv \frac{h^{-3\alpha/n}}{3\alpha\,\Gamma(3\alpha)}. \tag{31}$$

Let $s = \frac{3\alpha}{n} - 1$. When $s > 0$ (i.e., $3\alpha/n > 1$), the correction term vanishes as $r \to 0$, yielding $f(r) \to 1$. Here, the metric is regular at the origin in the g_{tt}-component, whereas for the Schwarzschild solution $f_{\text{Sch}}(r) \to -\infty$ as $r \to 0$.

In its standard formulation, the Dymnikova regular black hole metric takes the form

$$f_{\text{Dym}}(r) = 1 - \frac{2M}{r}\left[1 - e^{-r^3/r_0^3}\right]. \tag{32}$$

or, more generally, with a mass function $m_{\text{Dym}}(r)$ that varies smoothly from 0 at the center to M as $r \to \infty$. The present

model falls within the same qualitative category, characterized by a monotonically increasing mass function $m(r)$ satisfying

$$\lim_{r\to 0} m(r) = 0 \quad (\text{if } 3\alpha/n > 0), \qquad \lim_{r\to\infty} m(r) = M. \tag{33}$$

Hence, both geometries remove the central singularity by introducing an extended core in place of the point mass. The main distinction arises in the radial dependence: Dymnikova's profile exhibits exponential suppression, while our model follows an Einasto-like form involving the lower incomplete gamma function, producing a power-law behavior at small r controlled by α and n. Since the mass function $m(r)$ monotonically grows from a small central value to the total mass M at spatial infinity, three distinct qualitative configurations emerge, determined by the parameters (M, α, n, h):

1. Two horizons (inner and outer), analogous to non-extremal regular black holes.
2. One degenerate horizon (extremal configuration).
3. No horizon, if $2\,m(r) < r$ for all $r > 0$, producing a horizonless compact object.

Unlike the present model, the Schwarzschild solution features a single, non-degenerate event horizon at $r = 2\,M$.

3.2.1 Consistency: Ricci scalar

The Ricci scalar for the above system can be written as

$$R = -8\pi\left(4\rho + r\rho'\right) = -8\pi\rho_0 e^{-x(r)}\left(4 - \frac{x(r)}{\alpha}\right), \tag{34}$$

which remains finite at $r = 0$ and vanishes asymptotically, confirming the regular nature of the fuzzified Dymnikova black hole.

4 Energy conditions

We first recall the definitions of the energy conditions in component form for a diagonal stress tensor:

- **Null Energy Condition (NEC)**: for any null vector k^μ,

  $$T_{\mu\nu}k^\mu k^\nu \geq 0 \implies \sigma + p_i \geq 0 \quad (i = r, \theta, \phi).$$

  For spherical symmetry, it suffices to check

  $$\sigma + p_r \geq 0, \qquad \sigma + p_\perp \geq 0.$$

- **Weak Energy Condition (WEC)**: for any timelike vector u^μ,

  $$T_{\mu\nu}u^\mu u^\nu \geq 0 \implies \sigma \geq 0,\ \sigma + p_i \geq 0 \quad (i = r, \perp).$$

- **Strong Energy Condition (SEC)**: for any timelike vector u^μ,

  $$\left(T_{\mu\nu} - \tfrac{1}{2}T g_{\mu\nu}\right)u^\mu u^\nu \geq 0$$

  which for a diagonal anisotropic fluid is equivalent to the pair of inequalities

  $$\sigma + p_i \geq 0 \quad (i = r, \perp), \qquad \sigma + p_r + 2p_\perp \geq 0.$$

- **Dominant Energy Condition (DEC)**: in addition to the WEC, the energy flux is causal, which for a diagonal stress tensor reduces to

  $$\sigma \geq |p_i| \quad (i = r, \perp).$$

Analysis for the fuzzified Dymnikova model.

Using $p_r = -\sigma$, we have

$$\sigma + p_r = \sigma - \sigma = 0,$$

for all r. Hence, the radial combinations are marginal (saturating to zero).

For the tangential combination,

$$\sigma + p_\perp = \sigma - \sigma\left(1 + \frac{x}{2\alpha}\right) = -\frac{x}{2\alpha}\,\sigma(r).$$

Since $x(r) \geq 0$ and $\sigma(r) \geq 0$, it follows that

$$\sigma + p_\perp = -\frac{x}{2\alpha}\,\sigma(r) \leq 0,$$

with equality only at the center $r = 0$, where $x(0) = 0$.

Finally, the SEC combination reads

$$\begin{aligned}\sigma + p_r + 2p_\perp &= \sigma - \sigma + 2\Big(-\sigma - \frac{x}{2\alpha}\sigma\Big)\\ &= -2\sigma\left(1 + \frac{x}{2\alpha}\right) \leq 0,\end{aligned}$$

which is strictly negative for any $r > 0$.

The DEC inequalities are

$$\sigma \geq |p_r| = \sigma \quad (\text{saturated}), \qquad \sigma \geq |p_\perp| = \sigma\left(1 + \frac{x}{2\alpha}\right).$$

Thus, the DEC holds as illustrated in Fig. 4.

Physical interpretation The core of the fuzzified Dymnikova geometry is *vacuum-like*: as $r \to 0$, $p_r \simeq p_\perp \simeq -\sigma_0$ and the stress mimics a de Sitter vacuum (cosmological-constant behaviour). In that sense the radial equation-of-state $p_r = -\sigma$ is vacuum-like and marginally satisfies $\sigma + p_r = 0$. However the tangential pressure is more negative (because

of the slope term $r\sigma'/2$), producing anisotropy and leading to violations of the usual energy conditions away from the centre. Such violations are common and expected in models that regularize the central singularity (they are typically interpreted as effective contributions from quantum vacuum polarization or exotic/DE-like matter rather than ordinary classical matter).

Analysis

- At $r = 0$ one has $x(0) = 0$, hence $p_r(0) = p_\perp(0) = -\sigma_0$; all marginal inequalities are saturated there (e.g. $\rho + p_i = 0$).
- For small but nonzero r, the tangential violation scales like $-\frac{x}{2n}\sigma \sim -\frac{1}{2n}(r/r_s)^{1/n}\sigma_0$, so the violation is mild near the core and grows outward according to the Einasto index n.
- If desired, one can plot $\sigma + p_\perp, \sigma + p_r$ and $\rho + p_r + 2p_\perp$ to illustrate the regions of violation for chosen parameter values (σ_0, r_s, α).

In the presented fuzzified stellar model, we noted that the radial component of the fluid fulfills all conventional energy conditions, such as NEC, WEC, SEC, and DEC, whereas the tangential component violates them for $r > 0$. The anisotropic stress distribution together with the EDP function, which is necessary to maintain regular, non-singular interiors, naturally leads to these violations. This kind of behavior represents the unusual stress-energy structure necessary to support the generalized Dymnikova black-hole or horizonless stellar configurations and to avoid singularity development, rather than suggesting a physical instability of the overall arrangement. The non-local EoS further guarantees a physically feasible and self-consistent structure, while the anisotropy stabilizes the situation by counteracting the gravitational force. As a result, these energy requirement violations are fundamental to the creation of our regular, smeared self-gravitational black solutions and have a significant physical relevance.

5 Relativistic effective potential

To examine the motion of test particles in the gravitational field of the fuzzified Dymnikova regular black hole, we study the relativistic effective potential derived from the underlying spacetime geometry. In his context, we test the astrophysical relevance of our model by exploring whether the proposed smeared DM solution can account for the central black hole of the Milky Way, characterized by a mass $M_{\rm BH} = 4.1 \times 10^6\, M_\odot$ and a Schwarzschild radius $R_{\rm BH} = 17.4\, R_\odot$ [76,77]. To proceed, it is necessary to obtain reliable estimates for the key parameters characterizing the smeared solution. In particular, we determine the model parameters by imposing that the total mass M and the mass $m(r)$ approximates $M_{\rm BH}$ when evaluated at the radius $r_{\rm min}$ corresponding to the minimum of the effective potential for massive test particles. That is,

$$1 - \frac{r_{\rm min}}{M_{\rm BH}} \leq 10^{-2}, \tag{35}$$

$$\frac{\dot{r}^2}{2} + \Phi^{\rm eff}(r) = \text{constant}. \tag{36}$$

Here, the overdot represents differentiation with respect to the proper time for massive particles, or with respect to an affine parameter in the case of massless particles. Accordingly, the effective potential associated with the fuzzified Dymnikova metric takes the form

$$\Phi^{\rm eff} = \frac{L^2}{2r^2} - \frac{\gamma(3\alpha, x)}{\Gamma(3\alpha)}\left(\frac{L^2}{r^3} - \frac{\varepsilon}{r}\right), \tag{37}$$

where $\varepsilon = 1$ for massive particles and $\varepsilon = 0$ for massless particles. Then, by introducing the rescaled parameters

$$u = \frac{r}{r_s}, \quad \mathscr{L} = \frac{L}{r_s}, \quad r_s = 2M_{\rm BH}. \tag{38}$$

we obtain

$$\Phi^{\rm eff} = \frac{\mathscr{L}^2}{2u^2} - \frac{\gamma(3\alpha, x(u))}{\Gamma(3\alpha)}\left(\frac{\mathscr{L}^2}{u^3} + \frac{\varepsilon}{2u}\right), \tag{39}$$

where $x(u) = \left(\frac{u}{H}\right)^{1/\alpha}$. On the other hand, the effective potential for the classical Schwarzschild metric is defined as

$$\Phi_{\rm S}^{\rm eff} = \frac{L^2}{2r^2} - \left(\frac{L^2}{r^3} - \frac{\varepsilon}{r}\right), \tag{40}$$

which by using Eq. (38), takes the form

$$\Phi_{\rm S}^{\rm eff} = \frac{\mathscr{L}^2}{2u^2} - \frac{\mathscr{L}^2}{2u^3} - \frac{\varepsilon}{2u}. \tag{41}$$

6 Discussion of graphical results

We now turn to the graphical examination of the principal physical parameters that characterize the Einasto-modified Dymnikova spacetime. The profiles of physical quantities $(\sigma, p_r, p_\perp, \Delta)$, metric potential $f(r)$, and the effective potential $\Phi_{\rm eff}(r)$ exhibit several physically significant features, which are summarized below.

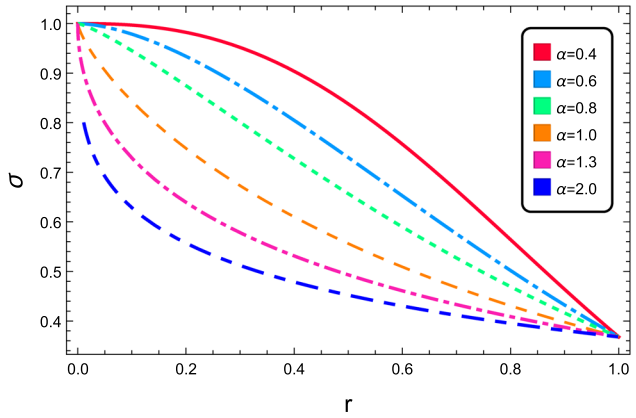

(a) Energy density $\sigma(r)$ for different α.

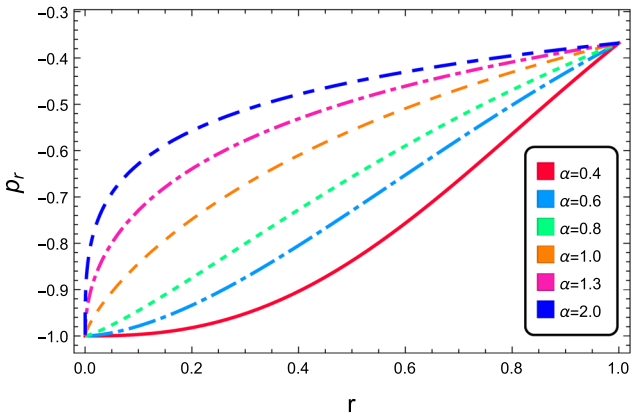

(b) Radial pressure $p_r(r)$ for different α.

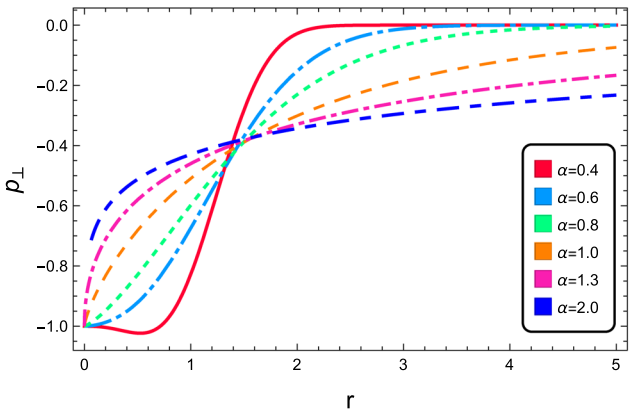

(c) Tangential pressure $p_\perp(r)$ for different α.

Fig. 1 Variation of the physical variables with r for different values of the Einasto index α

- **Energy Density:** The density profile $\sigma(r) = \sigma_0 e^{-x(r)}$ attains a finite maximum at the origin and decreases monotonically with increasing r, confirming a smooth, regular core structure without any singularities, as described in left panel of Fig. 1. The decay rate is governed by the Einasto index α; lower values of α correspond to a steeper and more centrally concentrated density profile, while higher α lead to a smoother and more extended core region.
- **Radial Pressure:** The radial pressure, defined as $p_r = -\sigma$, remains negative throughout the configuration, signifying a de Sitter–like repulsive core (see the right panel of Fig. 1). Its magnitude follows the same radial decay as the density and approaches zero asymptotically, ensuring that the spacetime is asymptotically Schwarzschild.
- **Tangential Pressure:** The tangential pressure, given by $p_\perp = -\sigma\left(1 + \frac{x}{2\alpha}\right)$, coincides with the p_r near the center but diverges at larger radii, indicating the onset of anisotropic stresses, as displayed by the bottom panel of 1. The deviation grows with radius but weakens for higher α, implying that the Einasto index regulates the level of anisotropy in the system. since $\sigma_0 > 0$ and $x(r) > 0$.
- **Anisotropy Factor:** The anisotropy factor $\Delta = p_\perp - p_r = -\frac{\sigma x}{2\alpha}$ vanishes at the center and becomes increas-

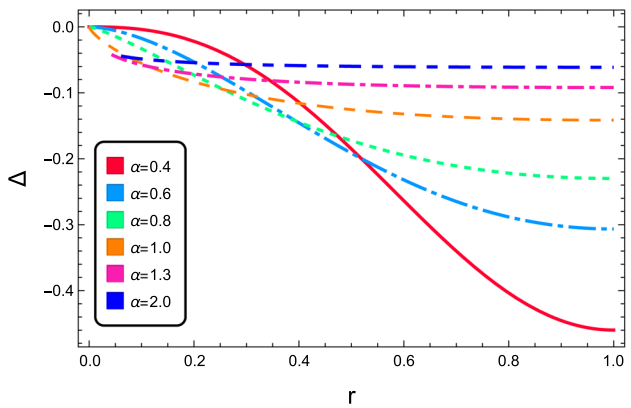

Fig. 2 Variation of the anisotropy parameter Δ with respect to r

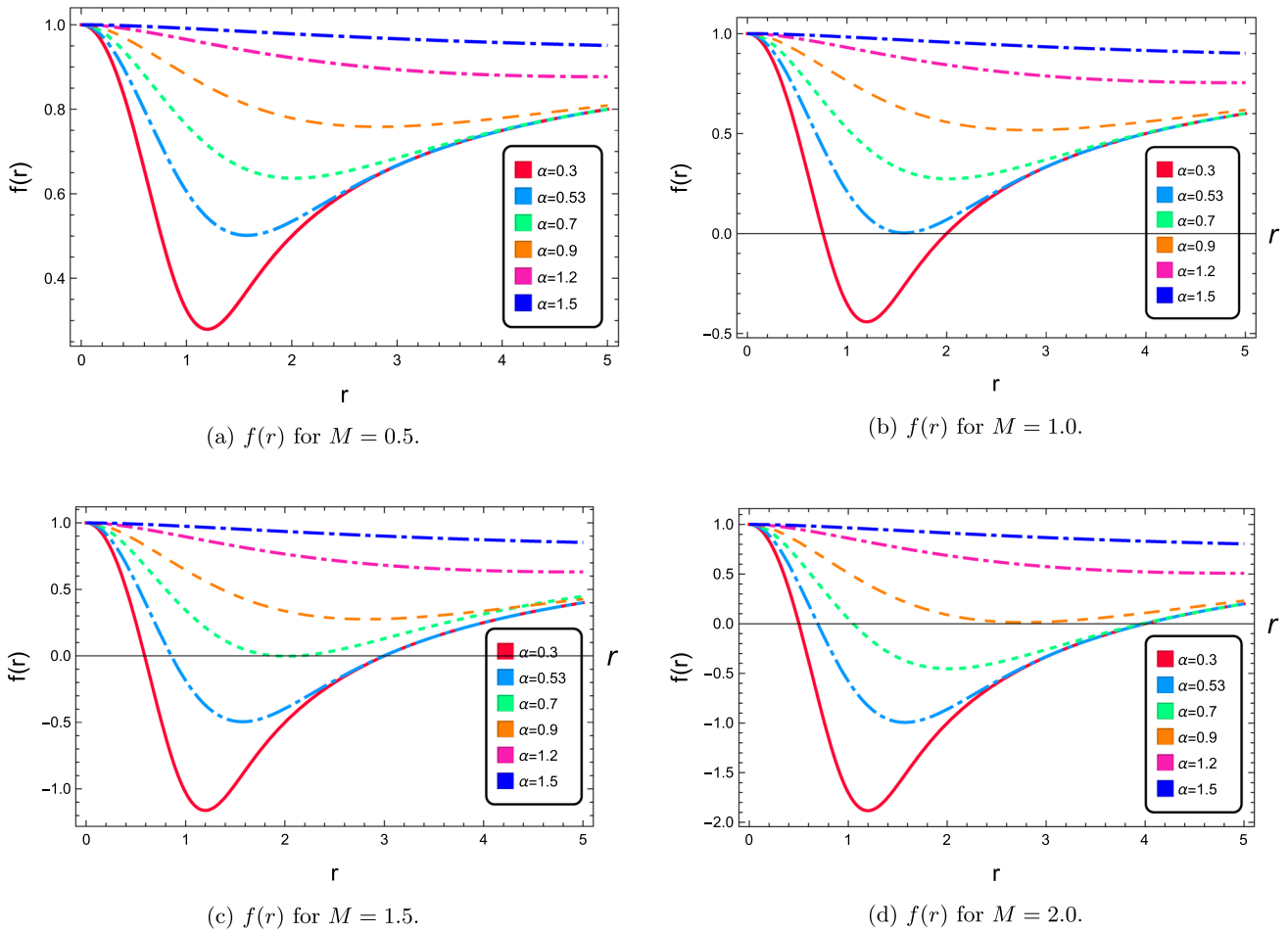

(a) $f(r)$ for $M = 0.5$. (b) $f(r)$ for $M = 1.0$.

(c) $f(r)$ for $M = 1.5$. (d) $f(r)$ for $M = 2.0$.

Fig. 3 Variation of the metric function $f(r)$ for different mass parameters M and Einasto indices α. Each panel illustrates the influence of α on the shape and horizon structure of the fuzzified Dymnikova black hole

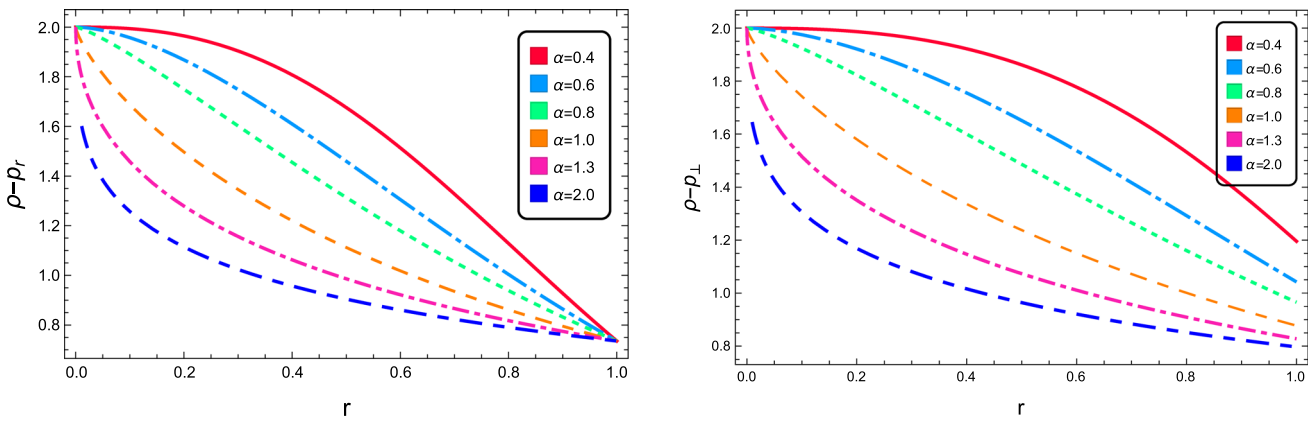

(a) DEC (b) DEC

Fig. 4 Variation of the DEC with respect to r

ingly negative outward (see Fig. 2). This indicates that the tangential pressure dominates over the radial one in magnitude beyond the core region. The anisotropy plays a crucial role in balancing gravitational attraction and internal pressure, thereby influencing the stability of the configuration. A negative value of Δ implies that $p_\perp < p_r$, that is, the tangential pressure is smaller than the radial one. The anisotropy vanishes at the center ($r = 0$) because

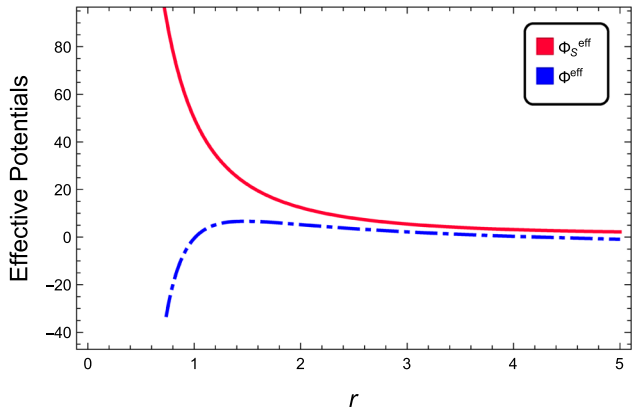

(a) $\Phi_{\text{eff}}(r)$ for massive particles ($\varepsilon = 1$), $\mathscr{L} = 10$, $H = 10$.

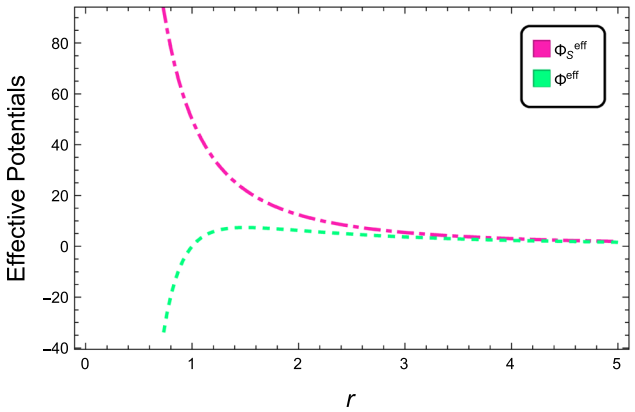

(b) $\Phi_{\text{eff}}(r)$ for massless particles ($\varepsilon = 0$), $\mathscr{L} = 15$, $H = 15$.

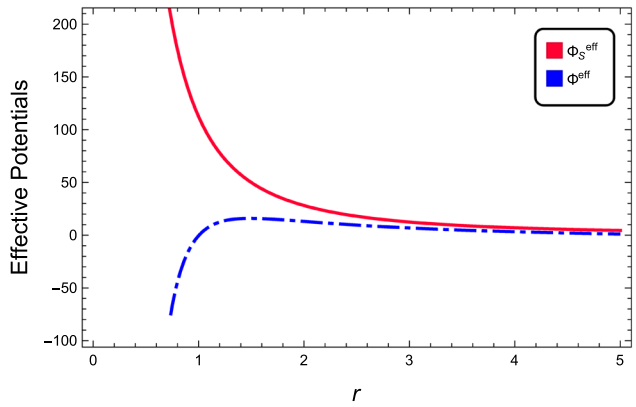

(c) $\Phi_{\text{eff}}(r)$ for massive particles, $\mathscr{L} = 20$, $H = 20$.

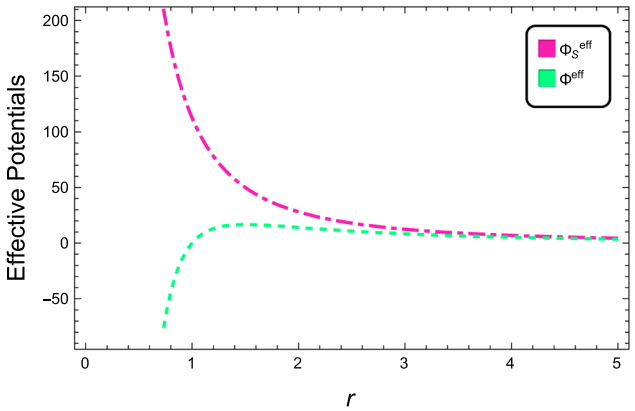

(d) $\Phi_{\text{eff}}(r)$ for massless particles, $\mathscr{L} = 10$, $H = 10$.

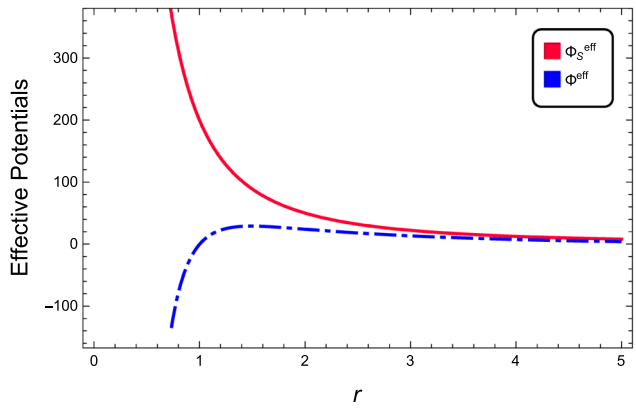

(e) $\Phi_{\text{eff}}(r)$ for massive particles, $\mathscr{L} = 15$, $H = 15$.

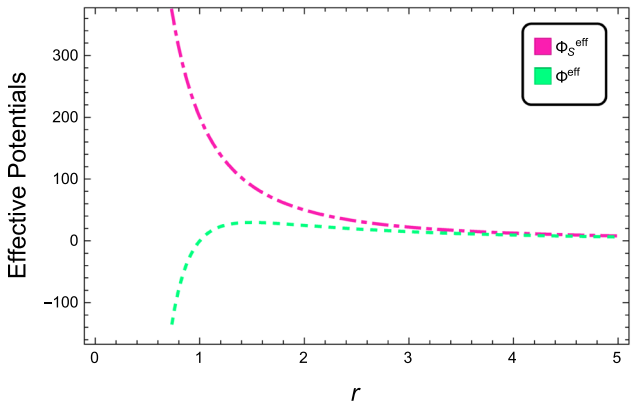

(f) $\Phi_{\text{eff}}(r)$ for massless particles, $\mathscr{L} = 20$, $H = 20$.

Fig. 5 Plots of the effective potential with respect to r

$x(0) = 0$. Hence, the anisotropy increases outward, suggesting that the fluid becomes progressively more underpressured in the tangential direction compared to the radial one.

- **Metric Function:** The metric potential $f(r)$ remains finite and positive inside the core, confirming the regularity of the spacetime. Depending on the chosen parameters, the metric may describe a regular black hole with one or two horizons, or a horizonless compact droplet. Increasing the Einasto index α produces a smoother transition from the de Sitter-like interior to the Schwarzschild exterior geometry. The intersections with the horizontal axis correspond to the radii of the event horizons. For $\alpha = 0.53$ and $M = 0.5$, a single degenerate horizon exists (dash-dotted line) (see Fig. 3). When $\alpha = 0.3$ and $M = 0.5$ (solid line), two distinct horizons appear.

However, for $\alpha > 0.53$, the solution becomes horizonless, representing an anisotropic stellar droplet. A similar qualitative behavior of the metric function is observed for higher mass values $M = 1.0,\ 1.5$, and 2.0.

- **Effective Potential:** To investigate stable and unstable orbits of the model, the graphical behavior of the effective potential Φ^{eff} for test particles has been examined. As seen in Fig. 5, the profile of Φ^{eff} depending on the parameter selections is very similar to the traditional Schwarzschild case, with some significant changes around the core area because of the fuzzified geometry. The ordinary black hole admits stable circular orbits around it, whose characteristics depend on the parameter α, as evidenced by the presence of a distinct minimum in the effective potential (Fig. 4).

7 Summary

Considering the cosmic abundance of DM, we employed the Einasto density model to construct a well-behaved self-gravitating configuration representing DM-inspired black holes within Einstein's general relativity (Fig. 5). In particular, we developed an Einasto profile–based generalization of the Dymnikova regular black hole metric. The proposed method yields a family of compact stellar models that remain finite at the core and recover known solutions for specific parameter values. This framework thus established a coherent link between two of the most intriguing cosmic entities: black holes and DM. We have demonstrated that by tuning the mass and shape index parameters of the Einasto density distribution, one can construct a variety of self-gravitational configurations, including regular black holes and horizonless compact objects. The detailed investigation of the physical parameters of the model highlights the viability of these DM-motivated stellar structures.

Key Findings:

1. The Shape parameter α associated with Einasto density distribution acts as a control parameter, regulating the degree of regularity and compactness of the resulting geometry.
2. The generalized Dymnikova–Einasto metric produces stable, non-singular configurations that can represent either fuzzy DM droplets or regular black holes with one or two horizons.
3. The effective potential for test-particle motion closely resembles that of the Schwarzschild black hole under appropriate parameter conditions, ensuring physically consistent trajectories.
4. The analysis of the standard energy conditions (NEC, WEC, SEC, and DEC) reveals that the model marginally satisfies the radial components while violating the tangential ones for $r > 0$. Specifically, the null and weak energy conditions are saturated at the center but violated away from it, whereas the strong and dominant energy conditions are not fulfilled throughout the spacetime. This behavior is consistent with the regular nature of the solution, where such violations are typically required to prevent singularity formation.
5. Small deviations in the potential profiles across different parameter sets can serve as diagnostic tools to distinguish among competing fuzzy black hole models.
6. The shadow structure predicted by this model offers an observable signature that could be tested through the Event Horizon Telescope and related experiments.

To determine their unique optical and observational signals, future studies will concentrate on a thorough examination of the gravitational lensing properties linked to the Einasto-based regular self-gravitational solutions.

Acknowledgements This research has been funded by Scientific Research Deanship at University of Ha'il, Saudi Arabia through project number.

Data Availability Statement This manuscript has no associated data or the data will not be deposited. [Authors' Comment: This manuscript contains no associated data.]

Code Availability Statement The manuscript has no associated code/software. [Author's comment: Code/Software sharing not applicable to this article as no code/software was generated or analysed during the current study.]

Declarations

Conflict of interest The authors have no Conflict of interest with respect to the publication of the present paper.

Open Access This article is licensed under a Creative Commons Attribution 4.0 International License, which permits use, sharing, adaptation, distribution and reproduction in any medium or format, as long as you give appropriate credit to the original author(s) and the source, provide a link to the Creative Commons licence, and indicate if changes were made. The images or other third party material in this article are included in the article's Creative Commons licence, unless indicated otherwise in a credit line to the material. If material is not included in the article's Creative Commons licence and your intended use is not permitted by statutory regulation or exceeds the permitted use, you will need to obtain permission directly from the copyright holder. To view a copy of this licence, visit http://creativecommons.org/licenses/by/4.0/.
Funded by SCOAP[3].

References

1. C.S. Frenk, S.D. White, Ann. Phys. **524**, 507 (2012)
2. A. Del Popolo, M. Le Delliou, Galaxies **5**, 17 (2017)

3. J.F. Navarro, C.S. Frenk, S.D.M. White, Astrophys. J. **490**, 493 (1997)
4. B. Moore et al., Mon. Not. R. Astron. Soc. **310**, 1147 (1999)
5. A.D. Cintio et al., Mon. Not. R. Astron. Soc. **441**, 2986 (2014)
6. A. Burkert, Astrophys. J. **447**, L25 (1995)
7. G. de Vaucouleurs, Ann. Astrophys. **11**, 247 (1948)
8. W. Jaffe, Mon. Not. R. Astron. Soc. **202**, 995 (1983)
9. S. Khan, H.M.A. Mahmoud, Phys. Dark Universe **49**, 102053 (2025)
10. J. Wagner, Gen. Relativ. Gravit. **52**, 61 (2020)
11. H. Zhao, Mon. Not. R. Astron. Soc. **278**, 488 (1996)
12. E.L. Łokas, G.A. Mamon, Mon. Not. R. Astron. Soc. **321**, 155 (2001)
13. N. Evans, J. An, Mon. Not. R. Astron. Soc. **360**, 492 (2005)
14. J.L. Feng, Annu. Rev. Astron. Astrophys. **48**, 495 (2010)
15. W. Hu, R. Barkana, A. Gruzinov, Phys. Rev. Lett. **85**, 1158 (2000)
16. Z. Yousaf, Phys. Dark Universe **48**, 101884 (2025)
17. H.-Y. Schive, T. Chiueh, T. Broadhurst, Nat. Phys. **10**, 496 (2014)
18. P. Mocz, M. Vogelsberger, V.H. Robles, J. Zavala, M. Boylan-Kolchin, A. Fialkov, L. Hernquist, Mon. Not. R. Astron. Soc. **471**, 4559 (2017)
19. J. Veltmaat, J.C. Niemeyer, B. Schwabe, Phys. Rev. D **98**, 043509 (2018)
20. B. Schwabe, J.C. Niemeyer, Phys. Rev. Lett. **128**, 181301 (2022)
21. B. Schwabe, J.C. Niemeyer, J.F. Engels, Phys. Rev. D **94**, 043513 (2016)
22. D. Levkov, A. Panin, I. Tkachev, Phys. Rev. Lett. **121**, 151301 (2018)
23. J. Chen, X. Du, E.W. Lentz, D.J. Marsh, J.C. Niemeyer, Phys. Rev. D **104**, 083022 (2021)
24. J.F. Navarro, E. Hayashi, C. Power et al., Mon. Not. R. Astron. Soc. **349**, 1039 (2004)
25. D. Merritt, J.F. Navarro, A. Ludlow, A. Jenkins, Astrophys. J. **624**, L85 (2005)
26. J. Einasto, Tr. Astrofiz. Inst. Alma-Ata p. 87 (1965)
27. J. Einasto, Astrophysics **5**, 67 (1969)
28. G.A. Mamon, E.L. Lokas, Mon. Not. R. Astron. Soc. **362**, 95 (2005)
29. V.F. Cardone, E. Piedipalumbo, C. Tortora, Mon. Not. R. Astron. Soc. **358**, 1325 (2005)
30. D. Merritt, A.W. Graham, B. Moore, J. Diemand, B. Terzić, Astron. J. **132**, 2685 (2006)
31. G.A. Mamon, A. Biviano, G. Murante, Astron. Astrophys. **520**, A30 (2010)
32. B.K. Dhar, L.L. Williams, Mon. Not. R. Astron. Soc. **405**, 340 (2010)
33. Z. Yousaf et al., Phys. Dark Universe **46**, 101629 (2024)
34. A.M. Albalahi, Z. Yousaf, A. Ali, S. Khan, Eur. Phys. J. C **84**, 9 (2024)
35. S. Khan, Z. Yousaf, Phys. Scr. **99**, 055303 (2024)
36. A.M. Albalahi, Z. Yousaf, S. Khan, A. Ali, Eur. Phys. J. C **84**, 963 (2024)
37. N. Iqbal, S. Khan, M. Alshammari, W.W. Mohammed, M. Ilyas, Eur. Phys. J. C **85**, 372 (2025)
38. H.M.A. Mahmoud, S. Khan, L.M. Abdalgadir, Phys. Dark Universe **49**, 101974 (2025)
39. M. Alshammari, H. Aman, et al., Int. J. Geom. Methods Mod. Phys. https://doi.org/10.1142/S0219887826500428 (2025)
40. S. Khan, Z. Yousaf, Phys. Scr. **99**, 095304 (2024)
41. S. Khan, A. Adeel, Z. Yousaf, Eur. Phys. J. C **84**, 572 (2024)
42. N. Loewer, M. Tayde, P. Sahoo, Eur. Phys. J. C **84**, 1196 (2024)
43. Z. Hassan, G. Mustafa, P.K. Sahoo, Symmetry **13**, 1260 (2021)
44. P. Moraes, P. Sahoo, Eur. Phys. J. C **77**, 480 (2017)
45. D. Mohanty, S. Ghosh, P. Sahoo, Phys. Dark Universe **46**, 101692 (2024)
46. M. Tayde, Z. Hassan, P. Sahoo, Phys. Dark Universe **42**, 101288 (2023)
47. L. Herrera, N.O. Santos, Phys. Rep. **286**, 53 (1997)
48. L. Herrera, Phys. Rev. D **101**, 104024 (2020)
49. A. Sokolov, Sov. Phys. JETP **52**, 575 (1980)
50. N.K. Glendenning, Phys. Rev. D **46**, 1274 (1992)
51. S. Khan, J. Rayimbaev, I. Ibragimov, S. Muminov, A. Dauletov, A. Abdujabbarov, Phys. Scr. **100**, 085302 (2025)
52. E. Battista, V. De Falco, Eur. Phys. J. C **82**, 628 (2022)
53. E. Battista, H.C. Steinacker, Eur. Phys. J. C **82**, 909 (2022)
54. E. Battista, Phys. Rev. D **109**, 026004 (2024)
55. S. Capozziello, S. De Bianchi, E. Battista, Phys. Rev. D **109**, 104060 (2024)
56. N. Iqbal, S. Khan, M. Alshammari, W.M. Mohammed, M. Ilyas, Eur. Phys. J. C **85**, 1336 (2025)
57. E. Hayashi, S.D.M. White, Mon. Not. R. Astron. Soc. **388** (2008)
58. E. Retana-Montenegro, E. Van Hese, G. Gentile, M. Baes, F. Frutos-Alfaro, Astron. Astrophys. **540**, A70 (2012)
59. J. Einasto, Astron. Nachr. **291**, 97 (1969)
60. L. Chemin, W.J.G. De Blok, G.A. Mamon, Astron. J. **142**, 109 (2011)
61. D. Batic, D.A. Abuhejleh, M. Nowakowski, Eur. Phys. J. C **81**, 777 (2021)
62. D. Batic, J.M. Faraji, M. Nowakowski, Eur. Phys. J. C **82**, 759 (2022)
63. Z. Yousaf et al., Chin. J. Phys. **88**, 406 (2024)
64. Z. Yousaf et al., Chin. J. Phys. **45**, 4345 (2025)
65. S. Khan, J. Rayimbaev, I. Ibragimov, S. Muminov, A. Dauletov, Ann. Phys. 170130 (2025)
66. L. Gao et al., Mon. Not. R. Astron. Soc. **387**, 536 (2008)
67. V. Springel, S.D.M. White, A. Jenkins et al., Nature **435**, 629 (2005)
68. B.K. Dhar, L.L. Williams, Mon. Not. R. Astron. Soc. **427**, 204 (2012)
69. I. Dymnikova, Gen. Relativ. Gravit. **24**, 235 (1992)
70. E.B. Gliner, Sov. J. Exp. Theor. Phys. **22**, 378 (1966)
71. E. Gliner, Sov. Phys. Dokl. **15**, 559 (1970)
72. I.G. Dymnikova, Int. J. Mod. Phys. D 529 (1996)
73. S. Haouat, K. Nouicer, Phys. Rev. D **89**, 105030 (2014)
74. Y.C. Ong, Eur. Phys. J. C **80**, 777 (2020)
75. R. Casadio, A. Giusti, J. Ovalle, J. High Energy Phys. **2023** (2023)
76. A.M. Ghez et al., Astrophys. J. **620**, 744 (2005)
77. A.M. Ghez et al., Astrophys. J. **689**, 1044 (2008)